

# An Integrated Study of the Dynamics of Electromagnetic and Acoustic Regimes During Failure of Complex Macrosystems Using Rock Blocks

Kamel Baddari · Anatoly D. Frolov ·  
Victor Tourtchine · Fayçal Rahmoune

Received: 20 October 2010 / Accepted: 14 December 2010 / Published online: 28 December 2010  
© Springer-Verlag 2010

**Abstract** The development of the failure process in complex macrosystems using large rock samples subjected to biaxial compression has been studied by means of electromagnetic radiation (EMR) and acoustic emission (AE). In order to increase the stage of macrofailure development, a special procedure of rock loading was used to reveal regularities of nucleation and evolution of electromagnetic and acoustic structures. The synchronised measurements of EMR and AE allowed the control of the stress–strain state in the rocks and the structural developments of fracturing. Non-homogeneous distribution of the rock spatial crystalline structure subject to load leads to a mosaic distribution of EMR and AE characteristics. As a result, the crack scale effect may be observed in the EMR and AE structure behaviours. The EMR and AE following the failure at different levels behave differently according to the difference in the scale and type of cracks. Intense high-frequency EMR pulses were recorded during the initial stage of microcrack generation occurring prior to major failure of material. This was not the case for AE. The nucleation and development of the macroscopic progressive failure evolution caused an alternation in energetic and frequencial properties of

electromagnetic and acoustic events. It has been detected that the tensile cracks were more efficient than shear cracks in capacity of EMR generation. The analysis of self potentials allowed reaching the maximum of registered anomalous variations in the stage of microcracking interaction. This stage showed an increase in the EMR activity, which implies the nucleation of microcracks in various regions of rock interfaces. The gradual accumulation of these defects led to weakening some parts of the rock along with a disintegration of electric anomalies, increase of AE and a significant fluctuation in the rate of EMR. When crack concentration attains its critical value, which results in the formation of dangerous macroscopic failure of higher level, AE shows an intense activity as well as an EMR lower frequency. The hierarchical development of rock failure using the ratio of the average crack size and the mean distance between cracks as a statistical concentration criterion is used to control the boundary of the transition from small dispersed cracks accumulation to gradual crack merger and the formation of the main macrofailure. These results could be transferred into larger scale levels to forecast dynamic events in the earth crust.

---

K. Baddari (✉)  
Laboratory of Physics of the Earth,  
UMBB, Boumerdes, Algeria  
e-mail: doyenfs@umbb.dz

A. D. Frolov  
SCEC, 64 Leninsky Pr. Russian Academy of Sciences,  
Moscow, Russia

K. Baddari · V. Tourtchine · F. Rahmoune  
Department of Physics, UMBB, Boumerdes, Algeria

K. Baddari · V. Tourtchine · F. Rahmoune  
Laboratory LIMOSE, UMBB, Boumerdes, Algeria

**Keywords** Physical subsystems · Space crystalline structure · Defects · Heterogeneity

## 1 Introduction

The physical subsystems associated with the spatial crystalline structure of any rock as a complex macrosystem and conditioning the response to external mechanical influences are ionic, dipolar, and electronic holes. The changes in the spatial structure are accompanied by some changes in mechanical, electrical and other physical properties of

the medium, most of which can be recorded by remote sensing methods.

Laboratory experiments (Anastasiadis et al. 2004; Bahat et al. 2005; Gong et al. 2006) showed the existence of electromagnetic radiation (EMR), which is emitted from loaded rocks. Recently, it was noticed that EMR, as short-term precursor, was observed frequently before some mine rockbursts and large earthquakes (Eftaxias 2010; Frid and Vozoff 2005; Pulinetes and Boyarchuk 2004; Sobolev and Demin 1980). To explain the recorded EMR associated with the rock failure at different scales, different effects have been suggested as probable physical mechanism of EMR pulse generation, among them, the electron emission during crystal fragmentation at the crack tip (Cress et al. 1987; Greiling and Obermeyer 2010), the relative movement of polarized crack (Freund and Sornette 2007; Makhmudov and Kuksenko 2005; Soloviev and Spivak 2009), the movement of electric charges (Mizuno and Mizuno 2002; O'Keefe and Thiel 1995), the atomic or ionic oscillations on the crack surface (Devyatkin et al. 2009; Frid et al. 2003; Gong et al. 2006), the piezoelectric effect (Gernets et al. 2004; Ogawa and Udata 2000; Wan and Hong 2008), and the semiconductor effect (Liu et al. 1997).

Acoustic emission by rock samples during failure reflects the process of crack formation and can be considered, most probably, as an analogue of global seismicity (Baddari et al. 1999; Dresen et al. 2010; Sobolev 1995; Xu et al. 2009). New possibilities for studying the behaviour of acoustic pulses during macrofailure preparation are available with more sensitive equipment to acoustic events (Fortin et al. 2006; Kuksenko et al. 2009; Lockner and Stanchits 2002, Smirnov et al. 2010). These studies and others describe the characteristic space–time–energy distributions of the AE in rock samples and indicate certain structural properties of AE which are quantitatively and qualitatively similar to the seismic regime. Thus, the experimental data on AE consolidate the physical basis of earthquake and rockburst prediction. Nevertheless, the experimental investigations on the EMR during rock failure are not as important as those of AE.

The purpose of this paper is to present experimental results about the synchronised measurements of EMR and AE to establish a correlation between the two emissions during the stages of nucleation, development and manifestation of the failure in rock blocks under load.

## 2 Kinetics of the Failure Growth in Heterogeneous Rock Blocks

The following physical factors are considered to be the basis of the failure process and the associated release of electromagnetic and acoustic energy: (1) the strain–stress

state in solids, including rocks, is far from being uniform, but it is a thermo-activation process in space and time and can, sometimes, be anisotropic, which makes the deformed rock mass state control much more difficult. (2) Whatever the rock, it is always characterized by a defined space crystalline structure with some strength distribution of grain contacts, grains and inter-grain zones. The structural development of rock deformation is accompanied by regular changes of these distributions caused by destruction of some less strong contacts, grains and formation of microcracks. The solid rock crack evolution in time depends on its heterogeneity, which has a determinant effect at all levels and could be followed at different clouds of a long process. (3) Failure is a hierarchical stochastic process. The existence of hierarchical levels may be explained by the fact that entropy in a quasi-closed system tends towards a maximum value (Bashkarev et al. 2002; Vettegren et al. 2004). The hierarchical levels exist in systems of objects of different sizes from the graininess samples of laboratory to the earth crust blocks.

The development of defects of nanometric sizes leads to the formation of microfracture. Nanodefects also fill multilevel hierarchy (Vettegren et al. 2003). The evolution of the crack is controlled by the stability and interaction of ruptures in the stress–strain field. The transition from the phase of the chaotic microcracks accumulation to the phase of local macrocrack may be explained by the following statistical approach. Consider a chaotic distribution of  $N_i$  cracks of size  $d$  in a volume  $V$  of a rock sample. If the mean distance  $\langle x \rangle$  between cracks in a loaded rock volume is expressed in terms of size  $d$  of cracks that are formed in this volume, the transition to macrocrack can reach a threshold microcrack concentration (Baddari et al. 1996; Kuksenko 2005; Sobolev and Ponomarev 2003; Zavyalov 2006), when

$$\frac{\langle x \rangle}{d} = \frac{X^{-1/3}}{d} = K \quad (1)$$

where  $X$  is the microcrack concentration. The parameter  $K$  characterizes the mutual interaction of cracks and their ability to merge via local stress field.

The probability  $P_n$  when the concentration of chaotic cracks attains a critical concentration  $X_c$  value and forms  $n$  cluster of adjacent cracks is expressed as

$$P_n = \frac{y^n}{n!} \quad (2)$$

Here, the mean number of cracks in the cluster is

$$y = \frac{n}{K} \quad (3)$$

Using Sterling formula

$$n! = \frac{n^n \sqrt{2 \pi n}}{e^n} \quad (4)$$

we obtain for  $n \gg 1$

$$P_n = \frac{y^n e^n}{n^n \sqrt{2 \pi n}} \tag{5}$$

If  $n \rightarrow +\infty$ ,  $\log P_n$  gives

$$\text{Log } P_n = n(1 - \log K) = \log \left(\frac{e}{K}\right)^n \tag{6}$$

so

$$P_n = \left(\frac{e}{K}\right)^n \tag{7}$$

where  $e$  is the natural logarithm base.

For  $K > e$  in Eq. 1, the appearance of the microcracks is feasible. On the contrary, this probability of microcracks appearance increases when  $K < e$ .  $K = e = 2.7$  constitutes the threshold of the migration of the rock from the chaotic distribution phase of the first hierarchical non-interacting microcracks to the active interaction for triggering a cluster and giving rise to the macrocracks in next level (Zavyalov 2005). These cracks accumulate until their concentration reaches again a critical value, which results in the formation of a greater rank level according to the same mechanism. Then, the transition from a low level to a higher one suggests a time sequence in the evolution of the 1st, 2nd, 3rd, ...,  $n$ th rank levels and occurs when the crucial concentration  $X_c$  of cracks of appropriate dimensions is attained in the failure focus.

Nevertheless, the decrease of  $K$  leads to the increase of the consolidation of cracks in order to give rise to more important cracks. During the chaotic distribution of microcracks inside a volume  $V$  of a rock under loading, the progress from sub-microcracks to larger level cracks can be studied using parameter  $K$ .

We suggest that EMR is radiated in association with microcrack growth. The motion of the microcrack extremities during their opening, leads to an emission in the maximum range of frequency

$$f = \frac{1}{t_T} \tag{8}$$

where  $t_T$  represents the duration of cracks opening. The value of  $t_T$  is determined by the crack size  $d$  and the speed of its nucleation  $v_T$

$$t_T = \frac{d}{v_T} \tag{9}$$

Alternately, if we suppose that EMR is generated by the sources near the crack extremities, the electric field of an elementary dipole with a polarization  $\mathbf{P}$  is given by the formula (Morgounov and Malzev 2007):

$$E = \frac{1}{4\pi\epsilon_0} \frac{1}{r^3} \left( 3 \frac{(\mathbf{Pr})r}{r^2} - \mathbf{P} \right) \tag{10}$$

where  $\mathbf{r}$  is a vector position from the dipole to the antenna. The polarization density  $\mathbf{p}$  at an arbitrary point is  $dP = p(x, y, z) dV$  (11)

here  $dV$  is the differential of volume of rock sample. The electric field at the antenna is

$$E = \frac{1}{4\pi\epsilon_0} \int_V \frac{1}{r^3} \left( 3 \frac{(\mathbf{p}(x, y, z)r)r}{r^2} - \mathbf{p}(x, y, z) \right) dV \tag{12}$$

and the polarized part of the rock block is characterized by a nonzero dipole moment  $\mathbf{p}$ . The modulus of the electric field recorded by the antenna is equal to

$$|E| \approx \frac{|p|}{\epsilon_0} \tag{13}$$

The power of obtaining one crack is (Gokhberg et al. 1995)

$$W_0 = \frac{2}{3c^3} \left(\frac{p}{t_T^2}\right)^2 = \frac{2}{3c^3} (q_0 \Omega t_T v_T^3)^2 \tag{14}$$

where  $q$  is the charge density at the crack extremities and  $\Omega$  is the ratio of the crack opening size (or the displacement of shear crack) in relation to the crack length. The power of the EMR per unit volume of a rock is

$$W = W_0 \gamma t_T \tag{15}$$

where  $\gamma$  is the speed of the formation of the crack depending on the rheology of the rock and the strain speed. We suppose that the total crack does not give rise to a number of cracks which is greater than  $N_{\max}$  and that the number of formed cracks is proportional to the deformation; hence we can write

$$\gamma = \frac{(N_{\max} \epsilon)}{(t \epsilon_{\max})} \tag{16}$$

where  $t$  is the duration of the deformation  $\epsilon$ ,  $\epsilon_{\max}$  the deformation corresponding to the macrofailure. Thus, the power of emission per unit volume is determined by the charge density over the crack extremities, the speed of deformation depending on the dimensions of the produced cracks, not on the frequency of emission.

The EMR emitted during the nucleation and the expansion of local mechanical instability in the deformed rock volume can be explained by the formation of charged dislocations, electrokinetics phenomena, dislocation and discharge processes and other physical mechanisms.

### 3 Experimental Methodology

The experimental studies were conducted on large-size rock samples, each one with dimensions of  $450 \times 450 \times 210$  mm; two stress concentrators were introduced under

an angle of  $40^\circ$  with respect to the vertical pressure axis  $P$  in order to favour shear failure (Fig. 1). Samples of diabase (E1), olivine (E2), granite (E3), basalt (E4) and concrete (E5) were subjected to a biaxial load. The lateral load  $H$  was maintained nearly constant (50 MPa). The vertical load  $P$  was changed according to three phases (Fig. 2a): (1) it was increased at a constant rate when the AE intensity was weak in the interval  $0-0.5 P/P_f$ ; (2) it was maintained constant, i.e. the loading rate was decreased with the AE growth over  $0.5-0.8 P/P_f$ ; (3) it was decreased according to the conservation of the constant AE intensity in the interval  $0.8-1 P/P_f$ , where  $P_f$  is the ultimate load value corresponding to rock macrofailure.

The total time of the experiment  $t_f$ , corresponding to the macrofailure appearance, has varied from 3 to 10 h with respect to the nature of each rock block. These experiments were carried out on a press with a servo control and AE rate feedback, which kept the AE intensity not higher than the chosen value. The particular load regime has an inverse coupling with AE: with the increase of the AE intensity, the speed of loading is diminished. A feedback between an AE pulse counter and the axial stress ensured a constant AE velocity throughout the test. Similar techniques were tested in special experiments of fracture propagation using samples of granite (Lockner et al. 1991; Thompson et al. 2006)

The EMR monitoring was performed using a block of magnetic antennas located near the lateral surface of the block at 0.5 m. The received signals are amplified and processed in a formation block. Regular frequency

characteristics of the signal reception chain in a tuning fork varied from 400 Hz to 3 MHz. These signals are then passed through a quadratic amplitude detector, from which the processed signal arrives to the block of analogue memory where its maximum amplitude is stored in an interval of 10  $\mu$ s. At the end of this period, a rectangular pulse of positive polarization of duration of 2–3  $\mu$ s is formed at the output of an electronic switch. Then, this pulse is directed to the analyser H/024-07 in order to obtain the energetic spectra of EMR. To eliminate disturbances on the energetic spectrum, an adjusted antenna over the frequency of 300 kHz is installed outside the block, where the sample is situated. The signals received by this antenna are amplified and compared to the threshold of the triggering off the installation reserved to produce an electric potential for the command block. If this potential happens, the command block does not transmit pulses to the electronic switch. Consequently, the undesired signals do not arrive at the input of the pulse analyser.

Acoustic signals were received by resonance PZT piezoelectric receivers of eigen frequency of 0.2 MHz. A special multi-channel system was used to record the wave forms. The block surfaces were covered with eight sensors linked to an input preamplifier, a high-frequency filter, an amplifier, a quadratic detector, a memory block, a control unit, an analyzer H/024-07, oscillographs GRS-6052 and a computer. This setup allowed us to eliminate the maximum of undesired signals. A transducer was fixed in the middle of the sample to serve as a controller of the organization of the inverse command of the piston pressure as well as a means to measure the loading being the function of the acoustic activity.

The loading was applied under the condition of invariability of the AE intensity. The AE activity used in the chain of the inverse command corresponded to the first dozens of events per second. Exceeding the AE rate activity has conducted immediately to a decrease in the axial load by the reduction of the motion speed of the piston pressure. The strain control regime was selected in accordance with the notion relative to the process occurring in the earthquake focal zones. The constant rate of stress 5 MPa/s and its possible variation during the test has allowed the control of the stability of the development of the macrofailure in the sample. The axial load was measured at the rate of 1 s intervals on a PC.

The recording of acoustic events was performed by recording, under numerical format, the time of first arrivals and first maximum amplitudes of signals of each transducer. The resolution of the numerical channel for the determination of the arrival time is of 0.04–0.05  $\mu$ s. To localise the AE sources, i.e. the crack formation points, a seismological technique was used to find out the hypocenter coordinates using the difference in AE signals

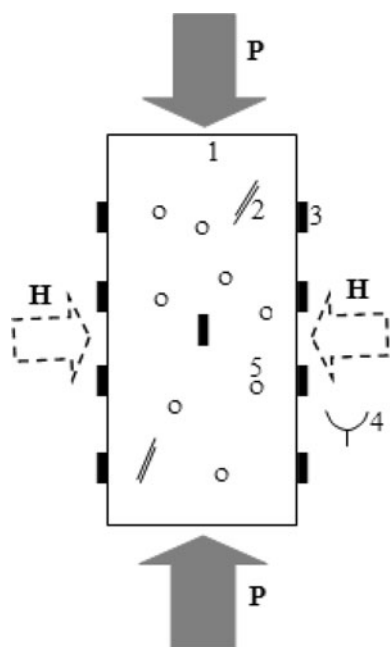
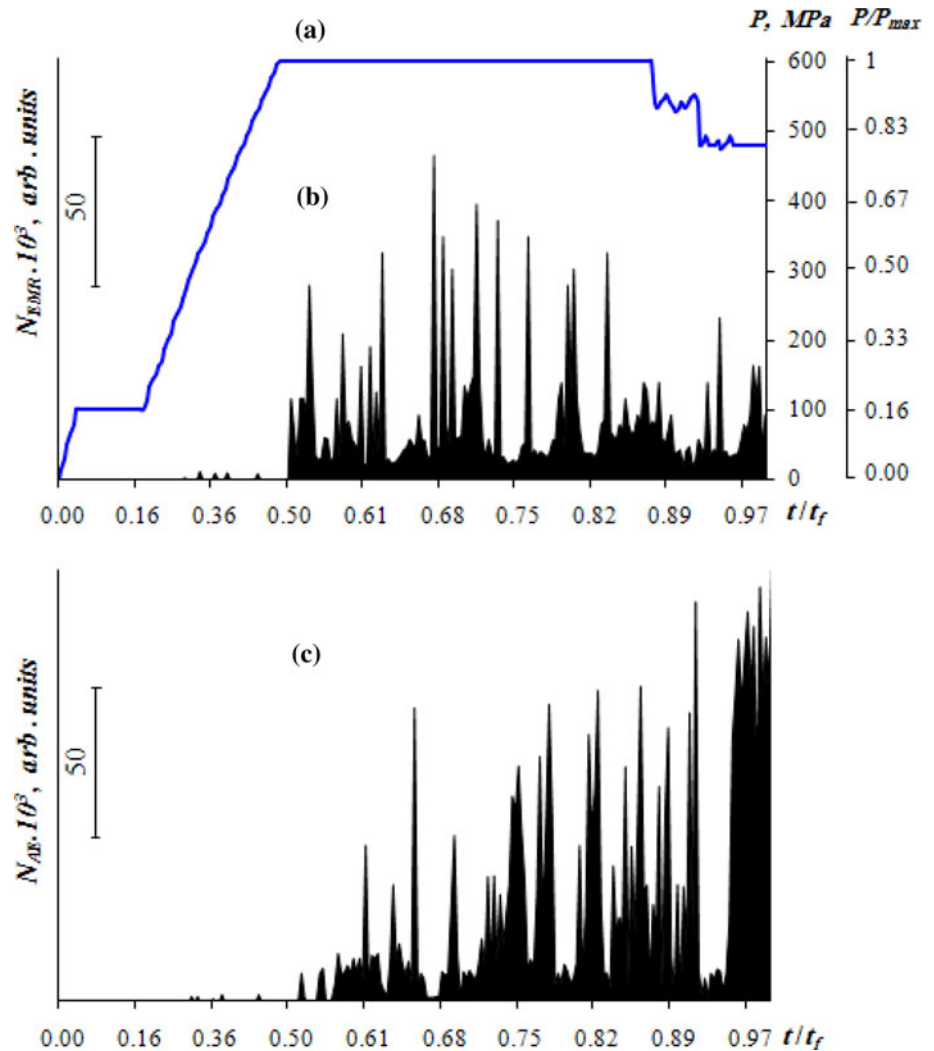


**Fig. 1** Schematic diagram of the experiment arrangement. 1 Pattern, 2 artificial stress concentrators, 3 acoustic emission sensors, 4 antenna, 5 self-potential electrodes,  $P$  main load,  $H$  intermediate load

**Fig. 2** Energy released spectra of EMR (a), AE (b) and the main load dependence (c) on time during the deformation of granite block



registration time. We have applied an algorithm using the time of first arrivals of longitudinal waves to the transducer and the minimum propagation time. The acoustic events having a propagation time greater than  $5 \mu\text{s}$  were eliminated from the AE catalogue. Nevertheless, the coordinates of the sources of AE was determined with an error of 1–1.5 mm according to the acoustic event value. The catalogue of the AE includes time, the Cartesian coordinates and the energetic class  $C$  ( $C = 2lgA$ , where  $A$  is the amplitude of the impulse in mV brought to a distance of 10 mm of the crack focus). The values of  $C_{\min}$  are 1.7, 2.0, 1.9, 1.8 and 1.5, respectively for the experiments E1, E2, E3, E5 and E4.  $A^2$  is proportional to event class energy  $C$ .  $C$  in this case is similar to the energy class used in seismology.

The elastic wave velocity was determined by four transducers whose propagation traces were directed according to the angles  $25^\circ$ ,  $50^\circ$  and  $70^\circ$  with respect to the vertical axis of the block. In this way, we have obtained 27,800–20,500 AE, 18,300–12,600 EMR, which is reliable

for experiments E1–E3 and 28,540–16,245 AE, 16,650–12,540 EMR for E4–E5. The amplitude of useful signals of EMR was recorded in a diapason 102–103 mV/m. The energetic evaluation was made based on the amplitude of the first maximum of the signal.

To study the structure of the electric field in detail, 15 nonpolarizable chlorine–silver electrodes were placed on the free faces of every rock block. The intrinsic drift of the electrode potentials did not exceed 0.7 mV during the experiment.

## 4 Experimental Results and Comments

### 4.1 Space and Time Regularities of EMR and AE

The most important emission activity was recorded in the influence zone of the stress concentrators where the shear crack was localised at the end of the experiment. An inequality in the intensities of AE and EMR was noted. The

acoustic and electromagnetic quiescences were recorded during different phases of block deformation. The visible frequency of pulses of AE and EMR are in the order of 300–400 kHz. Figure 2b, c gives a typical record of the total added released energy in 100 s interval of EMR and AE in the stress concentrators zone of the granite block. The quasi-elastic first phase corresponding to a gradual rise in differential loading is characterized by a low intensity of EMR and AE which begin to be recorded at the end of this phase at  $t/t_f = 0.45\text{--}0.5$  ( $t$  is the experimental time, named with respect to a total time  $t_f$  of the experiment), which reflects the beginning of weak microcracks process.

The stage from 0.5 to 0.8  $t/t_f$  is for the initiation of failure marked by large microcracks accumulation and is characterized by a rising in EMR and AE intensities. EMR was generated by oscillations of atom charges, considered as dipoles, after their bonds were ruptured. The set of excited dipoles between crack surfaces has developed a resultant dipole moment  $\langle p \rangle \neq 0$  (Eq. 13) and consequently an electric field. This is confirmed by the record of anomalous positive electric potential  $\Delta U$  in the interval 0.5–0.85  $t/t_f$  with a strong EMR. The non-uniformity of this intensity reflects the relaxation character in the variation of the stress concentration in the block which has been shared in robust and fragile zones.

As the block was deformed, the spontaneous electric field varied significantly. The microcrack intense evolution during the first stage of the stress–strain curve of the rock block is followed by an evolution of the electric potential. Maps of isopotential lines in the experiment E3 (Fig. 3) show examples of the evolution of local electric anomalies, when the load varied in the range 0.2–1  $t/t_f$ . One of these anomalies reached a maximum of about 45 mV at 0.7  $t/t_f$ , and then relaxed down to the background values over a period of several dozens minutes at 0.9  $t/t_f$ . The appearance of the anomaly coincided in time with the maximum of EMR and quiescence in AE.

At the time of loading  $t/t_f = 0.9\text{--}1.0$ , the variations of the surface electric field have significantly decreased. During this time, EMR remains practically constant. This indicates a relation between the EMR and electric anomalies. The dynamics of increase and of relaxation of electric potential  $\Delta U$  during the second stage and its correlation with the intense variation of EMR, in our opinion, reflects the microcracks accumulation process in the rock block.

Figure 4 shows variation of electric potentials of the electrodes 5 and 3 during the experiment E3. The potential increases at the beginning and decreases at the end of the experiment by about 50 mV. The increase of the potential corresponds to the beginning of the microcracks process. When  $\Delta U$  remains constant, we observe quiescence in EMR. A characteristic decrease of  $\Delta U$  was observed during

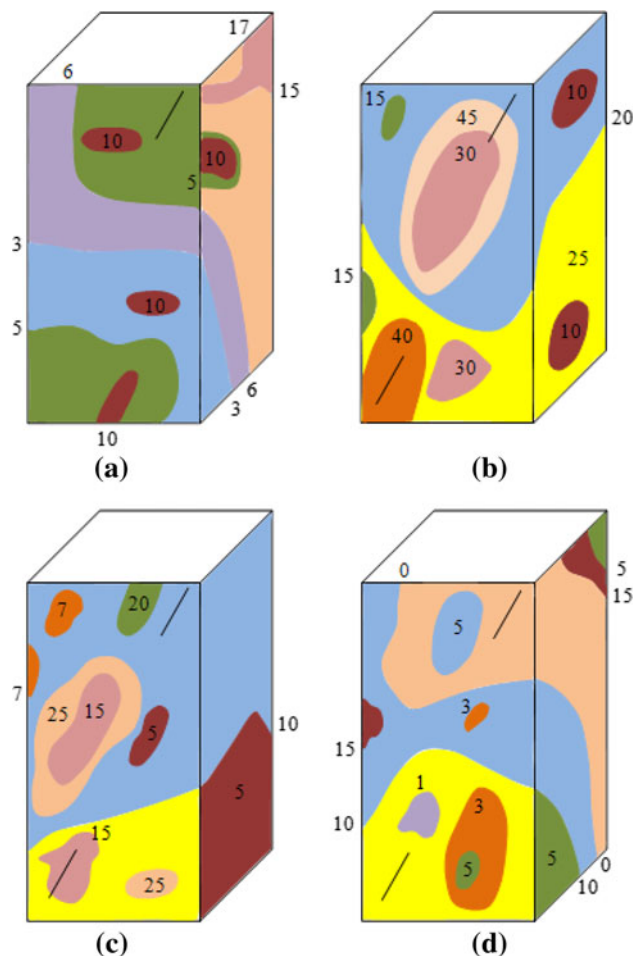


**Fig. 3** The isopotential contour maps for two planes I and III of the granite block, constructed for different time loading. **a** 0.2  $t/t_f$ , **b** 0.45–0.5  $t/t_f$ , **c** 0.7  $t/t_f$ , **d** 0.9–1  $t/t_f$ . Number at iso-lines represents potential value in mV, relative to zero electrode

the macrofailure stage at the end of the loading cycle. A number of features observed in the electric disturbances can be explained qualitatively within the framework of ionic migration mechanisms. The relaxation time of the electric charges arising at the failure surface makes it possible to record the EMR field through an antenna.

Figure 5 shows the ratio EMR/AE. Stage I of pre-maximal loading was marked at the end by a formation of small dispersive microcracks giving alternating tensile cracks oriented towards the main compressional stress. Stage II which is related to the maximum stress corresponds to an alternation of tensile and shear elements distributed non-uniformly through the block. The EMR intensity has initially decreased, but it is stronger than AE at the end of this stage. Stage III corresponds to the expansion of the shear lines to trigger off the shear cracks gradually. EMR marks relative quiescence during this stage compared to AE. Stage IV coincides with the expansion of shear cracks; few of them begin a sliding process leading to

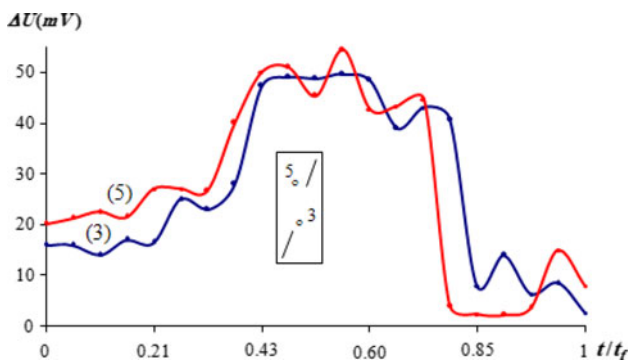


**Fig. 4** Variations of electric potential for the electrodes 3 and 5 in the experiment with the granite block

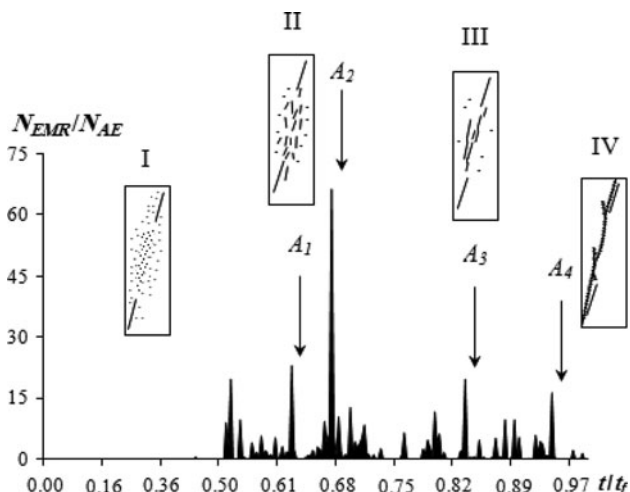


**Fig. 5** The ratio EMR/AE graph during the deformation of the rock granite block. Arrows A1–A4 correspond to moment of strong acoustic events

a progressive shear fracture of the rock sample. At this stage, an exponential increase of AE and relative decrease of EMR is noticed.

It should be observed that during the block deformation, four macrocracks occurred at the time of recording four strong acoustic events with the respective amplitudes 75, 80, 82 and 83 mV, preceded by a remarkable acoustic quiescence. The ratio EMR/AE shows the maximum corresponding to the triggering off these events.

The comparison of emission spectrum (Fig. 2b, c) shows that the high decrease of EMR is accompanied by the increase of the intensity of AE; on the contrary, during the acoustic silence, a high EMR is recorded. This is due to the emergence of microcracks having the same scale which is manifested in such emission. In this way, in the phase of isolated microcracks formation, a high intensity of EMR is recorded, compared to AE which remains low. Hence, we assist the creation of redundant electric charges isolated in space and variable in time over the crack extremities, while the elastic vibrations remain low.

The continued stress accumulation has led later to the unification of microcracks giving rise to macrocracks. When the mechanical energy of vibrations has become important, it has triggered off a maximum activity of AE, while EMR becomes low. This phenomenon is probably related to the electric charge compensation over the extremities of microcracks during the process of their multiplication.

The analysis of the amplitudes and the periods of signals of EMR and AE confirm this phenomenon. Indeed, at the formation phase of isolated microcracks, the amplitude and the pulse period of EMR are much greater than those of AE. The transition of the material to the third phase of deformation (the progressive macrofailure) triggers off a reverse relationship: the pulse quantity, as well as the amplitudes and periods (Fig. 6), increases highly. The relative power goes beyond the power of EMR. The increase of applied load on different rock blocks has led to changes in amplitudes and periods of AE (Fig. 6).

For diabase and granite materials (compared to basalt), the amplitudes of AE starts to go beyond the amplitudes of EMR for low relative stresses (deformations), while the pulse period of AE increases highly in the final phase of deformation. For concrete, such increase of amplitudes and periods is recorded mostly before the macrofailure. This difference is related to spatial crystalline structure which is different from the rock media and its evolution during their deformation process. It should be noted that the first signals of EMR and AE recorded simultaneously are short and have periods less than 500 μs. However, the signals of AE having periods less than 1 ms are not followed by similar signals of EMR.

Data analysis by an ultrasonic propagation device and by a microscope allowed to deduce that the short signals of AE are led by taking off cracks of lengths 0.5–2.5 mm, while long signals are emitted by shear cracks of length 12–35 mm. The latter ones seem not to have the capacity of triggering off an important EMR.

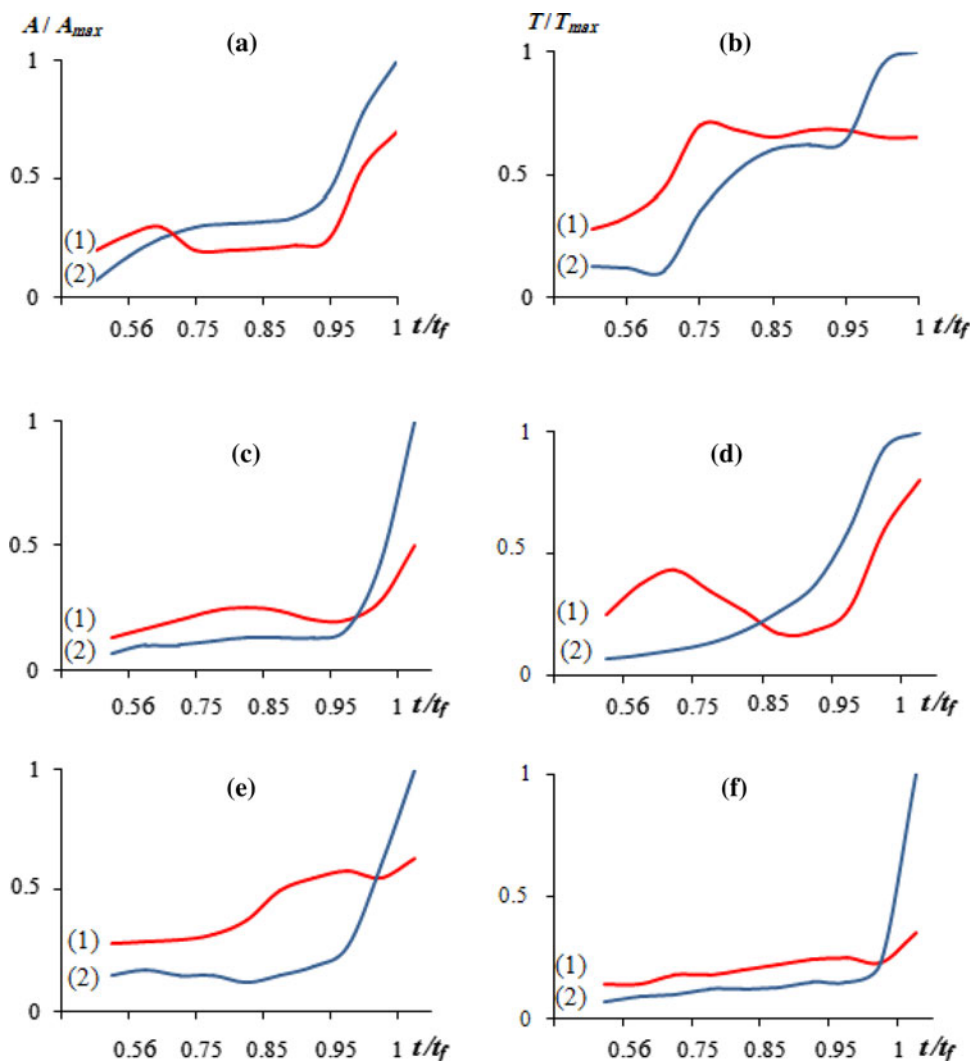
#### 4.2 Correlation between EMR and AE Dynamics and Cracks Dimensions

The seismogram analysis has allowed to calculate the length  $d$  of the crack, the duration  $t$  of source action and the propagation speed  $v$ . Figure 7a, b shows the variation  $d = f(t)$  and  $d = f(v)$ . The relation  $d = f(t)$  may be approximated by the function

$$d = 0.77e^{1.004t} \tag{17}$$

where  $t$  is measured in μs and  $d$  in cm. In the case of earthquakes  $t$  is in s and  $d$  in km (Sobolev and Ponomarev 2003). The length of failure has increased quickly with the velocity  $v$  of cracks evolution. The three phases of evolution of  $d$  are:

**Fig. 6** Variations of amplitudes and duration of emissions pulses. (1) EMR, (2) AE; **a**, **b** diabase; **c**, **d** basalt; **e**, **f** concrete



1.4–5, 5–11.9, and 11.9–25 cm. These give  $d_i/d_{i+1} = 2-3$ , which is in accordance with discrete geophysical medium (Sadovsky and Pisarenko 1991). When the failure reaches  $d = 25$  cm, the maximum correspondent velocity is 3.17 km/s which represents, in fact, the S wave velocity, knowing that the maximum recorded longitudinal velocity  $v_p$  in the experiment is 5.48 km/s ( $v_p = 1.73v_s$ ).

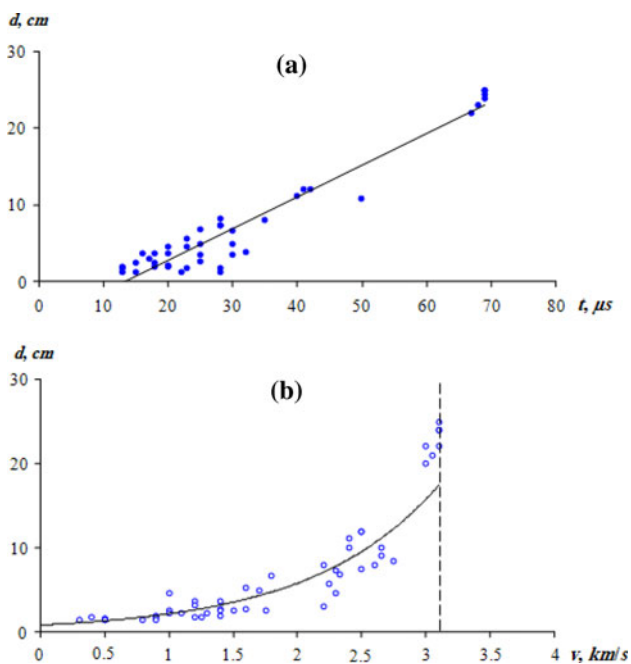
The experiments E3 and E4 have shown that the amplitude has changed from 6 to 150 mV for AE and from 10 to 140 mV for EMR. Indeed, the energetic class calculated by  $C = 2 \log a$ , where  $A$  is the amplitude of the pulse in mV,  $C = 1.55-4.35$  and  $C = 2-4.29$ , respectively for AE and EMR. The analysis of the recorded AE has allowed to classify  $C$  in three classes:  $C_1 = 1.55-2.20$ ,  $C_2 = 2.20-3.5$  and  $C_3 = 3.5-4.35$ , which correspond to three sizes of cracks  $d_1$ ,  $d_2$  and  $d_3$ . The corresponding number of AE and EMR has been recorded as follows:  $N_{AE}(C_1) = 27,330$ ,  $N_{AE}(C_2) = 3,805$ ,  $N_{AE}(C_3) = 420$  and  $N_{EMR}(C_1) = 20,795$ ,  $N_{EMR}(C_2) = 2,088$ ,  $N_{EMR}(C_3) = 32$ .

Figure 8a shows the variation of AE for the three classes  $C_1-C_3$  in the experiment E3. The existence of three phases of evolution of AE has been noted. Phase I corresponds to the random accumulation of microcracks during the stress growth. Phase II concerns the unification of microcracks and the beginning of the localisation of the macrofailure at the moment of constant stress. Phase III refers to the formation of the main macrofailure during the drop of the applied stress. A period of acoustic quiescence at  $t/t_f = 0.85$  has been recorded. The EMR (Fig. 8b) has shown an electromagnetic quiescence more visible and longer for  $C_1$  and  $C_2$  at  $t/t_f = 0.7-0.85$ , 10 min or more before that of AE.

The EMR of energetic class  $C_1$  confirms the three phases mentioned above: increase of electromagnetic activity, electromagnetic quiescence, and relatively short resumption of this activity before the macrofailure.

The EMR of class  $C_3$  remains practically low which confirms the hypothesis that the EMR is not sensitive to the generation of the principal macroshear failure of triggering





**Fig. 7** Rupture length’s dependence on action time source (a) and its propagation velocity (b). Dotted line indicates the maximum of S waves velocity

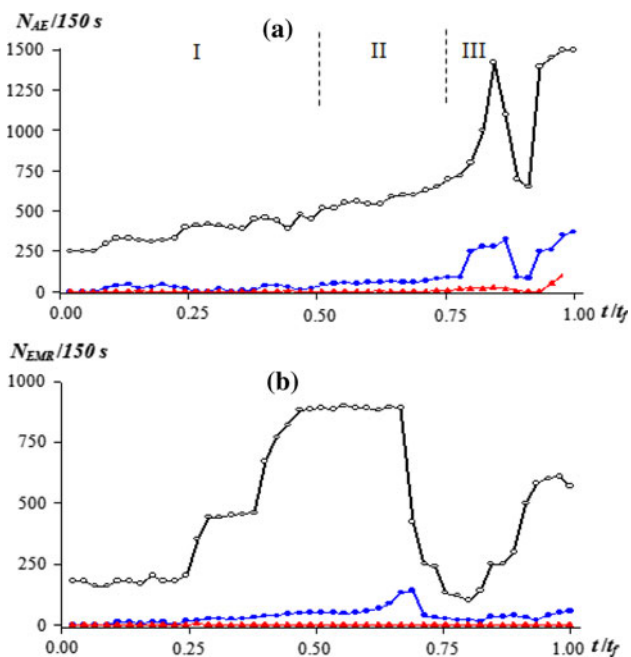


**Fig. 8** Variations of different energetic classes  $C$  of EA (a) and EMR (b) intensities during the formation of failure foyers in the experiment E3. Empty circle  $C_1$ , filled circle  $C_2$ , filled triangle  $C_3$

off at the end of the test. The size of rupture at phase III is greater than the one generated at phase II. Referring to the recursive formula of earthquakes (Sobolev and Ponomarev 2003)

$$\log N = a - b \log A \tag{18}$$

where  $a = 0.5$ ,  $A$  the amplitude and  $b$  characterizes the slope of the amplitude distributions, we can say that the number of cracks at phase III must be twice less than their number at phase II. Hence, the acoustic or electromagnetic quiescence is due to the phenomenon of unification of failures in order to produce a failure of higher rank. The second activation of AE and EMR is due to the frontier destruction between failures giving rise to the principal macrorupture.

The variation of  $b$  value shows clearly three distinct stages: a weak variation of  $b$  remained nearly constant around 1 in the interval  $0-0.5 t/t_f$ ; relative decrease of  $b$  value to 0.85 in the interval  $0.5-0.8 t/t_f$ ; and decrease of  $b$  value from 0.85 up to  $0.4-0.45$  starting from  $0.8-0.9 t/t_f$ . Based on the kinetic approach to the failure process, the decrease of  $b$  value is connected to the coalescence of failures and the formation of larger ones. An anomalous change in the slope of the recurrence curve can be regarded as a precursor of an approaching macrofailure (Carpinteri et al. 2009; Colombo et al. 2003; Rao and Lakschmi 2005; Yuan and Li 2009).

It should be noted that starting from  $t/t_f = 0.75-0.85$ , all the EMR and AE hypocenters have been localised in a narrow band of 7–10 mm thick. In order to study in details the structure of this band, the set of EMR and AE in the test E3 has been projected in a coordinate system  $x, y, z$ , so that  $x$  is perpendicular to the plane of maximum number of foyers of EMR and AE,  $z$  is situated in this plane and  $y$  forms an angle of  $90^\circ$  with this plane. The origin of this new system is situated on the axis of the block. The data base has been shared into two parts:  $\Pi_2$  with  $z \leq 10$  mm and  $\Pi_1$  with  $z > 10$  mm. Figure 9 shows that starting from  $t/t_f = 0.75$ , we record an antiphase variation of  $\Pi_2$  and  $\Pi_1$ . The increase of  $\Pi_2$  is followed by the decrease of  $\Pi_1$ , which explains the clustering of the foyers of AE and EMR in order to form the principal macrofailure of the block.

In order to study the clustering of AE, we have considered that at least two AE are clustered if the distance between their foyers and the time of their triggering off are less than their critical values, respectively (Baddari et al. 1996; Sobolev and Ponomarev 2003):

$$d_{cr} = 3d + 1.5 \tag{19}$$

and

$$t_{cr} (0.10e^{0.5C_i - C_{min}}) \tag{20}$$

where  $d$  is the dimension of the cracks equal to

$$\text{Log } d = a \text{Log } E + c. \tag{21}$$

The coefficient  $a$  determines the relationship between the crack length and the energy  $E$ , ( $a = 0.244$ ),  $c = -1.34$ ,

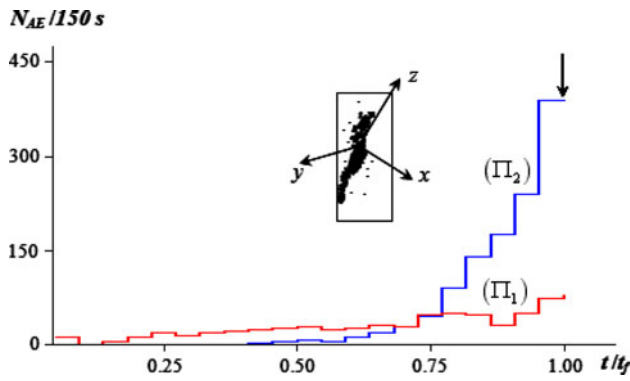


**Fig. 9** Variation of the AE activity inside ( $\Pi_2$ ) and outside ( $\Pi_1$ ) of failure zone. Arrow indicates the macrofailure initiation in the granite block

$C_{\min}$  the minima of the class energy in the experiment. The catalogue of all AE of different energies has shown that  $d_{cr} = 2\text{--}3.2$  mm;  $t_{cr} = 8\text{--}310$  s.

The experiments E1–E4 have shown the respective clustering of 5,218, 5,517, 3,065 and 1,284 acoustic events, which corresponds to 16; 9; 19.4 and 14.2% of the total recorded AE number. The experiments have shown that all the foyers of AE are generated or triggered off in a chaotic manner during the phase  $t/t_f = 0\text{--}0.75$  and are concentrated later in the future foyer of the macrofailure. The detailed study of the grouped AE of class  $C_3$  in the experiment E2 in the sphere of  $d_{cr} = 2.5\text{--}3$  mm has shown the recording of 358 AE of this type. Figure 8 shows a strong increase of grouped AE comparing to the isolated AE before the recording of AE of the considered class  $C_3$  in experiment E3. Hence, the macrofailure is followed by a grouping process of AE of higher energy due to the reconciliation of mutual cracks centres which increases their density and generates the magisterial rupture.

### 4.3 Cracks Concentration Parameter

We can suppose that the lifetime  $T$  of a rock under load is composed of two time phases, except the quasi-elastic stage: time phase I of duration  $T_{ac}$ , which corresponds to the microcracks accumulation; and time phase II of duration  $T_{pc}$ , which coincides with the clustering and progression of cracks to give the main failure. Therefore,  $T = T_{ac} + T_{pc}$ . The speed in the process of cracking in phase II is relatively higher than the one of phase I. Hence, we have  $T_{ac} \gg T_{pc}$ .

In order to use the parameter  $K$  to predict the macrofailure, we have considered Eq. 1, where  $X = N_i/V$  is the microcracks critical volumetric concentration of acoustic events in the rock volume  $V$  at the time  $t$ , and

$$d = \frac{I}{N_i} \sum_i^{N_i} l_i \tag{22}$$

is the mean length of crack in the cluster set, where:  $N_i$  is the number of acoustic events of energetic class  $[C_{\min} - C_{\max}]$  appearing in volume  $V$  during time  $t$ ,  $l_i$  the size of opening microcracks or the unity crack size.

Knowing that we did not measure the length of the formed crack  $l_i$  during the experiment, we have considered that the released energy  $E_i$  during the crack formation of size  $l$  is proportional to  $l_i^3$  (Baddari and Frolov 1997; Smirnov et al. 1995). Considering that  $E_i$  is proportional to  $A_i$ , where  $A_i$  is the amplitude of the acoustic pulse, we have applied

$$l_i = \beta A_i^{2/3} \tag{23}$$

where  $\beta$  is a constant coefficient.

By substituting  $d$ ,  $X$  and  $l_i$  (Eqs. 22–23) in Eq. 1, we obtain

$$K = \alpha \frac{N_i^{2/3}}{\sum_{i=1}^{N_i} A_i^{2/3}} \tag{24}$$

where  $\alpha = \frac{1}{\beta} V^{2/3}$ , which is unknown experimentally; thus we have used

$$K = \frac{N_i^{2/3}}{\sum_{i=1}^{N_i} A_i^{2/3}} \tag{25}$$

$K$  has varied in the experiment E3, according to this assumption, by three phases (Fig. 10). In phase I ( $K = 20\text{--}15$ ), the microcracks do not interact between them. In phase II, starting from  $t = 0.55\text{--}0.8 t/t_f$ , the process goes to the focal phase evolution corresponding to the formation of fractal structure related to the strain regime. The relative diminution of  $K$  is due to the accumulation of quasi-stationary defects in the peripheral domain of the future macrocrack. In phase III, in the

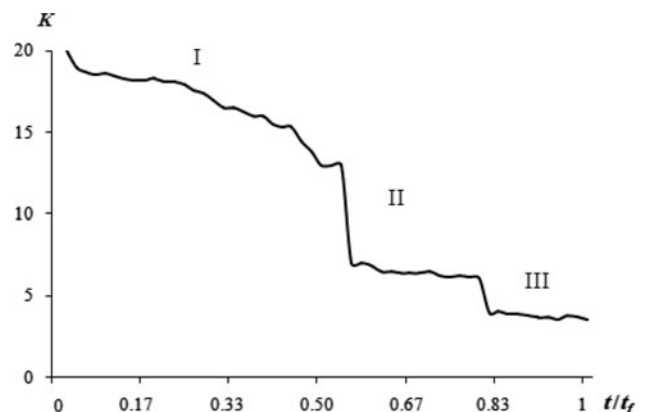


**Fig. 10** Changes in  $K$  parameter during the deformation of the basalt block

interval at  $t = 0.8-1 t/t_f$ ,  $K$  has decreased before the macrofailure and signals of high energy ( $A = 80-85$  mV) have been recorded, which corresponds to the formation of more important defects and to a progress of a macrocrack. This process continues in associated domains, giving rise at the end to the principal crack. During this phase, the density of cracking becomes critical ( $K \sim 5$ ) and the process of deformation migrates to an interaction stage, the system of microdefects of rank  $i$  loses its stability and more important defect of rank  $(i + 1)$  or more are triggered and thereby, we obtain a concentration of microdefects and a localisation of the macrocrack.

Note that the obtained threshold value of the parameter  $K$  exceeds 2.7 and may be explained by the use of the correlation relationship (Eq. 22) for calculating the average defect size. The interaction of defects is realised through stress field, which could be expressed statistically by the fact that a given acoustic event will change the probability of triggering off the next event, in a particular domain of space. The size of this domain is approximately equal to a radius  $R$  of defects interaction. If we admit that these defects interact when they reach the critical concentration  $X_c$ , it can be deduced that

$$R = K \quad (26)$$

In other way, we know that the ratio between the rupture stress  $P_r$  and the stress  $P_R$  at distance  $R$  is given by Sobolev (1995)

$$\frac{P_r}{P_R} = \left(\frac{R}{l}\right)^{1/2} \quad (27)$$

Therefore, the hierarchical accumulation and kinetics of failures at different scales obey the same law when the parameter  $K$  is principal to define the transition from one level to the following.

## 5 Conclusions

The variations of EMR and AE are due to the evolution of the failure process. The rate of increase in EMR is higher than the rate of change of AE during the first stage of the formation of primary cracks in the rock block. The exponential increase of AE is observed during the transition from delocalisation to localisation spells in cracks, giving a critical concentration which causes, at the end, a main fault.

The EMR and AE, following the micro and macrocracks of rocks at different phases of their deformation, differ by the tendency of their variations, conditioned by the difference in the scale of crack. The diminution of the intensity of the EMR is accompanied generally by an increase in the intensity of AE and vice versa. This is

related to the change of the disjunctive steps of the microcracks (maximum EMR) and the multiplication of these is followed by their clustering (maximum AE). This change characterizes the quasi-elastic phase and the progressive macrorupture phase which lead gradually to the formation of local macrocracks.

The presence of the EMR in the intervals of AE quiescence testifies the continuation of the concentration of the mechanical stress and the sub-deformation of the solid parts from the preparation zone of the local rupture, which will increase the reliability of its prediction. The final step of deformation of the rock generates an increase in the energy and the power of EMR and AE. The advanced growth of AE compared to EMR is a precursor of the local macrocracks. When reaching a critical concentration of cracks, the fusion leads to a formation of larger ones and is responsible of acoustic and low frequency electromagnetic radiation. We note that EMR is more sensitive to the generation of tensile cracks than shear cracks.

The synchronised record of EMR and AE and the interpretation of their spectra and their ratio represent a perspective to obtain information about the heterogeneity degree of the crack and the art of deformation of massive rocks at all scales. The evolution of the deformed hierarchical medium of solid complex crystalline blocks at different scales from nanodefects in microscopic grains to the faulting in the earth crust accompanied by dynamic events suggests that the development of the failure process is controlled by the same physical process.

## References

- Anastasiadis C, Triantis D, Stavrakas I et al (2004) Pressure stimulated currents (PSC) in marble samples. *Ann Geophys* 47(1):21–28
- Baddari K, Frolov A D (1997) Modeling of fractal structure of geophysical field. *CR Acad Sci Paris* 325, série IIA, 925–930
- Baddari K, Sobolev GA, Frolov AD (1996) Similarity in seismic precursors at different scales. *C R Acad Sci Paris* 323, série IIA, 755–763
- Baddari K, Sobolev GA, Frolov AD, Ponomarev AV (1999) An integrated study of physical precursors of failure in relation to earthquake prediction, using large scale rock blocks. *Ann Geophys* 42(5):771–787
- Bahat D, Rabinovitch A, Frid V (2005) Tensile fracturing in rocks. *Tectonofractographic and electromagnetic radiation methods*. Springer, Berlin, p 570p
- Bashkarev AYa, Vettegren VI, Svetlov VN (2002) Hierarchy of statistical ensembles of nanodefects on the surface pressurised molybdenum. *Fiz Tverd Tela* 44(7):1260–1265
- Carpinteri A, Lacidogna G, Puzzi S (2009) From criticality to final collapse: evolution of the b-value from 1.5 to 1.0. *Chaos. Solitons Fractals* 41:843–853
- Colombo S, Main IG, Forde MC (2003) Assessing damage of reinforced concrete beam using “b-value” analysis of acoustic emission signals. *J Mater Civil Eng ASCE* 15:280–286

- Cress GO, Brady BT, Rowell GA (1987) Sources of electromagnetic radiation from fracture of rock samples in the laboratory. *J Geophys Res Lett* 14:331–334
- Devyatkin EA, Simonov IV, Sirotnin AA (2009) On electromagnetic radiation under destruction of ultrathin glass fibers. *Mech Solids* 44(1):131–140
- Dresen G, Stanchits S, Rybacki E (2010) Borehole breakout evolution through acoustic emission location analysis. *Int J Rock Mech Min Sci* 47(3):426–435
- Eftaxias K (2010) Footprints of nonextensive Tsallis statics, self-similarity and universality in the preparation of the l'Aquila earthquake hidden in a pre-seismic EM emission. *Phys A* 389:133–140
- Fortin J, Stanchits S, Dresen G, Gué'guen Y (2006) Acoustic emission and velocities associated with the formation of compaction bands in sandstone. *J Geophys Res* 111, B10203. doi:10.1029/2005J003854
- Freund F, Sornette D (2007) Electromagnetic earthquake bursts and critical rupture of peroxy bond networks in rocks. *Tectonophysics* 431:33–47
- Frid V, Vozoff K (2005) Electromagnetic radiation induced by mining rock failure. *Int J Coal Geol* 64:57–65
- Frid V, Rabinovitch A, Bahat D (2003) Fracture induced electromagnetic radiation. *J Phys D* 36:1620–1628
- Gernets AA, Makarets MV, Koshevaya SV, Grimalsky VV, Juarez RD, Kotsarenko AN (2004) Electromagnetic emission caused by the fracturing of piezoelectric crystals with an arbitrarily orientated moving crack. *J Phys Chem Earth* 29(4/9):463–472
- Gokhberg MB, Morgounov VA, Pokhotelov OA (1995) Earthquake prediction. Seismo-electromagnetic phenomena. Gordon and Beach Publisher, pp 191
- Gong Q, Hu XY, Zhang SY et al (2006) Relationship between frequency of electromagnetic radiation induced by rock fracture and the elastic parameters. *Chin J Geophys Chin Ed* 49(5):1523–1528
- Greiling RO, Obermeyer H (2010) Natural electromagnetic radiation (EMR) and its application in structural geology and neotectonics. *J Geol Soc India* 75:278–288
- Kuksenko VS (2005) Diagnostic and forecasting of breakage of large-scale objects. *Phys Solid Earth* 45(5):812–816
- Kuksenko VS, Makhmudov KhF, Mansurov VA, Sultanov U, Rustamova MZ (2009) Changes in structure of natural heterogeneous materials under deformation. *J Min Sci* 45(4):355–358
- Liu YZ, Liu Y, Wang YS, Jin AZ, Fu JM, Cao JP (1997) The influencing factors and mechanisms of the electromagnetic radiation during rock fracture. *J Acta Seismol Sin* 19(4):418–425
- Lockner DA, Stanchits SA (2002) Untrained poroelastic response of sandstones to deviatoric stress change. *J Geophys Res* 107(12):2553. doi:10.1029/2001JB001460
- Lockner DA, Byerlee JD, Kuksenko V, Ponomarev A, Sidorin A (1991) Quasi-static fault growth and shear fracture energy in granite. *Nature* 350:39–42
- Makhmudov Kh F, Kuksenko VS (2005) Electromagnetic phenomena entailed by deformation and fracture of dielectric solids. *Phys Solid State* 47(5):882–885
- Mizuno Y, Mizuno T (2002) Photon emission from ice during fracture. *Jpn J Appl Phys Part 2 Lett* 41(2B):L209–L211
- Morgounov VA, Malzev SA (2007) A multiple fracture model of pre-seismic electromagnetic phenomena. *Tectonophysics* 431(1–4):61–72
- O'Keefe SG, Thiel DV (1995) A mechanism for the production of electromagnetic radiation during fracture of brittle materials. *Phys Earth Planet Inter* 89(1–2):127–135
- Ogawa T, Udata H (2000) Coseismic piezoelectric effects due to a dislocation (1): An analysis far and early-time field solution in a homogeneous whole space. *J Phys Earth Planet Inter* 12(3/4):273–288
- Pulinetes SA, Boyarchuk K (2004) Ionospheric precursors of earthquakes. Springer, Heidelberg, p 289p
- Rao MVMS, Lakschmi PKJ (2005) Analysis of b-value and improved b-value of acoustic emissions accompanying cock fracture. *Curr Sci* 80:1577–1582
- Sadovsky MA, Pisarenko VF (1991) Seismic process and the block medium. Nauka, Moscow, p 96p
- Smirnov VB, Ponomarev AV, Zavyalov AD (1995) Acoustic structure in rock samples and the seismic process. *Phys Solid Earth* 31(1):38–58
- Smirnov VB, Ponomarev AV, Bernard P, Patonin AV (2010) Regularities in transient modes in the seismic process according to the laboratory and natural modeling. *Izv Phys Solid Earth* 46(2):104–135
- Sobolev GA (1995) Fundamental of earthquake prediction. ERC, Moscow, p 161
- Sobolev GA, Demin VM (1980) Mechano-electrical phenomena in the Earth. Nauka, Moscow, pp 1–215
- Sobolev GA, Ponomarev AV (2003) Earthquake physics and precursors. Nauka, Moscow, p 270
- Soloviev SP, Spivak AA (2009) Electromagnetic signals generated by the electric polarization during the constrained deformation of rocks. *Izv Phys Earth* 45(4):347–355
- Thompson BD, Young RP, Lockner DA (2006) Fracture in westerly granite under AE feedback and constant strain rate loading: Nucleation, quasi-static propagation, and the transition to unstable fracture propagation. *Pure Appl Geophys* 163:995–1019
- Vettegren VI, Bashkarev AJa, Svetlov VN, Morozov GI (2003) Hierarchy of nano and microdefects at the surface of loaded metals, Rus. *J Phys Chem* 77(Suppl. 1):163–166
- Vettegren VI, Kuksenko VS, Tomilin NG, Kryuchkov MA (2004) Statistics of microcracks in hetero-geneous materials (Granites). *Phys Fiz Tverd Tela* 46(10):1293–1796
- Wan GX, Hong L (2008) Piezoelectric responses of brittle rock mass containing quartz to static stress and exploding stress wave respectively. *J Cent South Univ Technol* 15:344–349
- Xu SC, Feng XT, Chen BR (2009) Acoustic emission characteristics and mechanical behavior of skarn under uniaxial cyclic loading and unloading. *Controlling Seismic Hazard and Sustainable Development of Deep in Mines (RASIM7)*, vols 1 and 2, pp 435–440
- Yuan RF, Li HM (2009) Identification of the predictive information before rock mass failure based on b-value of ae events and its deficiency. *Controlling Seismic Hazard and Sustainable Development of Deep in Mines (RASIM7)*, vols 1 and 2, pp 1447–1450
- Zavyalov AD (2005) From the kinetic theory of strength and fracture concentration criterion to the seismogenic fracture density and earthquake forecasting. *Phys Solid State* 47(6):1034–1041
- Zavyalov AD (2006) Intermediate term earthquake prediction. Nauka, Moscow, p 254